Nanoscale

PAPER

View Article Online
View Journal | View Issue

Cite this: *Nanoscale*, 2014, **6**, 2238

Charge separation in Pt-decorated CdSe@CdS octapod nanocrystals†

Erika Conca,‡[a] Mauro Aresti,‡[b] Michele Saba,*[b] Maria Francesca Casula,[a] Francesco Quochi,[b] Guido Mula,[b] Danilo Loche,[a] Mee Rahn Kim,[c] Liberato Manna,[c] Anna Corrias,[a] Andrea Mura[b] and Giovanni Bongiovanni[b]

Received 18th October 2013
Accepted 26th November 2013

DOI: 10.1039/c3nr05567a

www.rsc.org/nanoscale

We synthesize colloidal CdSe@CdS octapod nanocrystals decorated with Pt domains, resulting in a metal–semiconductor heterostructure. We devise a protocol to control the growth of Pt on the CdS surface, realizing both a selective tipping and a non-selective coverage. Ultrafast optical spectroscopy, particularly femtosecond transient absorption, is employed to correlate the dynamics of optical excitations with the nanocrystal morphology. We find two regimes for capture of photoexcited electrons by Pt domains: a slow capture after energy relaxation in the semiconductor, occurring in tipped nanocrystals and resulting in large spatial separation of charges, and an ultrafast capture of hot electrons occurring in nanocrystals covered in Pt, where charge separation happens faster than energy relaxation and Auger recombination. Besides the relevance for fundamental materials science and control at the nanoscale, our nanocrystals may be employed in solar photocatalysis.

Introduction

Colloidal nanocrystals represent a promising platform for scalable, low-cost exploitation of solar energy through the realization of solution-processable solar cells and photocatalytic reactors.[1–3] Photoconversion functionalities with colloidal nanoparticles require a specific design of the interfaces, with particular regard to the creation of defects, dangling bonds and potential barriers that hinder the extraction of photoexcitations and their energy from nanocrystals.[4] A viable strategy to overcome limitations relies on the growth of colloidal nanostructures with junctions between domains of different materials, realizing the device functionality at the nanometric scale.[5–8] Such a strategy may prove especially valuable for solar water splitting, an application where several interfaces and vectorial charge transport are usually required.[1,4,9–12]

The choice of semiconductor materials for solar water splitting is subject to the fulfillment of thermodynamic requirements: the bandgap has to exceed the minimum 1.23 eV value, corresponding to the net free energy in the water splitting reaction, with the correct offset with respect to the vacuum level. CdS-based nanocrystals have the right level alignment and have been particularly amenable to the realization of complex shapes and heterostructures, like branched nanocrystals.[13,14] Multipod nanocrystals appear well suited for realization of complex optoelectronic functions needed in photocatalysis, as their topology may favor multiple step relaxation pathways for optical excitations. Recent advances in nanocrystal fabrication have managed to produce CdSe@CdS nanocrystals with up to 8 separate pods, realizing highly branched yet well-defined nanostructures.[15–17]

The fact that the water splitting reaction is energetically favorable does not imply that it will actually occur under solar illumination, due to the presence of activation barriers and kinetics bottlenecks. Catalysts are typically required for efficient photoconversion reactions and noble metals are the most widely used materials. Photocatalytic water splitting has been pursued with CdSe/CdS-based elongated nanocrystals decorated at the surface with noble metal domains, employing a variety of methods for nanocrystal decoration and resulting in different sizes, shapes and locations of the metal domains, both with selective noble metal deposition on the nanorod tips and a non-selective coverage of the nanocrystal surface.[18–31] A corresponding variety of electron transfer rates have been reported, but it is unclear whether complete surface coverage or selective tipping with noble metal domains is the most promising nanocrystal architecture because of a lack of direct comparison between heterostructures with equal composition and size obtained by the same synthesis route, highlighting a correlation between microscopic structure and optoelectronic function.

[a]*Dipartimento di Scienze Chimiche e Geologiche and INSTM, Università di Cagliari, Cittadella universitaria, I-09042 Monserrato, Italy*

[b]*Dipartimento di Fisica, Università di Cagliari, Cittadella universitaria, I-09042 Monserrato, Italy. E-mail: saba@unica.it*

[c]*Istituto Italiano di Tecnologia, via Morego 30, 16163 Genova, Italy*

† Electronic supplementary information (ESI) available: Octapod synthesis and decoration procedures, transient absorption spectroscopy experimental setup, and time-resolved photoluminescence experimental setup. See DOI: 10.1039/c3nr05567a

‡ These authors have contributed equally.

In this work, we demonstrate a method to control Pt deposition on CdSe@CdS octapod nanocrystals, realizing both a selective tipping and a non-selective surface coverage of the CdS surface with Pt nanoparticles. By means of ultrafast transient absorption, we investigate the consequences of different decorations on photophysical properties, in particular on the capture of photoexcited electrons by Pt domains, the initial step of photocatalytic reactions. We realize experimental conditions where the electron capture is fast enough to compete with energy relaxation, leading to the capture of hot electrons. Experiments under intense pulsed optical excitation reveal that Pt-decorated octapod nanocrystals are able to cause charge separation simultaneously for tens of photoexcitations.

Results and discussion

Octapod nanocrystals are grown through a colloidal route from a sphalerite CdSe core obtained by cation exchange of a $Cu_{2-x}Se$ seed.[16] TEM observations, as shown in Fig. 1, indicate that the octapods tend to lie on the substrate sitting on four arms and are homogeneous in shape and size, with average pod length and diameter of 48 nm and 12 nm, respectively. As shown by previous investigation, the octapod arms grow along the *c* axis due to the faster growth of the high-energy (0001) facet of the wurtzite structure. The metal–semiconductor interface is realized in a second step by decorating the octapod surface with Pt domains. We set the synthesis so that the dimensions of Pt nanoparticles do not depend on the concentration of precursors. The aim of the decoration procedure is to control the geometry of the attachment of Pt to the CdS surface, without varying the morphology of octapod nanocrystals nor that of Pt domains. The degree of Pt coverage of the CdS surface is controlled by the amount of Pt precursors in solution: low Pt concentrations result in a selective deposition of Pt only on the most reactive surfaces, *i.e.* on the pod tips (Fig. 1c); on the other hand, a five-fold increase in Pt concentration results in a non-selective, extensive Pt coverage of the entire pod surface (Fig. 1d). It should be pointed out that, as desired, in both Pt-tipped and Pt-covered CdSe@CdS heterostructures the size of the metal domains is around 3.5 nm. X-ray diffraction data in Fig. 2a reflect the occurrence of the anisotropic hexagonal CdS phase and peak broadening provides size estimates in agreement with what was inferred directly from TEM images, an indication that nanocrystals are mainly single crystalline domains. The main reflection of the Pt structure can be observed in the Pt-covered octapods, with average nanocrystal size 3.5 nm. Fig. 2b shows the effects of Pt decoration on the optical absorption: spectra for Pt-free octapods are characterized by a sharp absorption edge around 500 nm in wavelength, corresponding to the optical bandgap of CdS, followed by a Rayleigh diffusion tail; knowing the concentration of nanocrystals in dispersion, we determine the absorption cross-section to be $\sim 6 \times 10^{-13}$ cm^2 at 400 nm. When Pt is added, Rayleigh diffusion grows with the amount of Pt, as expected from plasmonic field enhancement effects. No clear plasmon resonance is however observed. The absorption cross-section does not appear to be significantly modified by the Pt decoration procedure; however, the limited quantities of Pt-decorated nanocrystals obtained after purification procedures have prevented an accurate determination of the concentration of nanocrystal dispersions and therefore uncertainties of the order of 30% need to be considered for the quantitative assessment of the absorption cross-section.

Large nanocrystals with a spatially controlled metal–semiconductor heterostructure represent a versatile playground for testing some of the photophysical processes relevant for solar photoconversion. CdSe/CdS heterostructured nanocrystals have a quasi-type II band alignment, with conduction bands almost aligned and the CdSe valence band higher in energy than the CdS one;[32–38] the relaxation paths of photoexcited electrons and holes are also influenced by the surface and interface morphology.[39–43] The photophysics of Pt-decorated nanocrystals is studied here with ultrafast optical spectroscopy, in particular

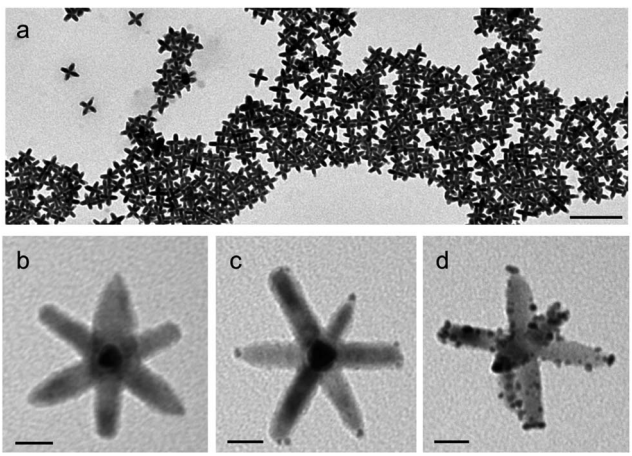

Fig. 1 (a) TEM image of an ensemble of CdSe@CdS octapod nanocrystals, highlighting the homogeneity in shape and size in the batch; the scale bar is 200 nm. Representative images of (b) a single Pt-free octapod nanocrystal, (c) a single Pt-tipped octapod nanocrystal and (d) a Pt-covered octapod nanocrystal. Scale bars in (b), (c) and (d) are 20 nm.

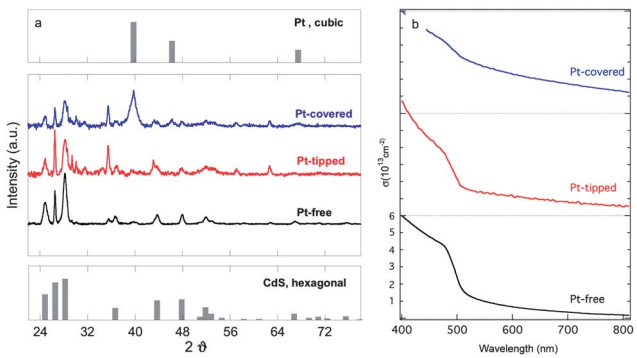

Fig. 2 (a) X-ray diffraction patterns of the Pt-free, Pt-tipped, and Pt-covered octapod nanocrystals. The diffraction peak position of the bulk CdS hexagonal and Pt cubic structures are reported on the bottom and on the top, respectively, as a reference. (b) UV-Vis absorbance measured in a toluene dispersion of Pt-free, Pt-tipped and Pt-covered octapod nanocrystals.

femtosecond transient absorption, a technique sensitive to the dynamics of the excited state.[44] In our case the excitation is provided by 150 fs-long laser pulses, 392 nm in wavelength, from a kHz repetition rate regenerative amplifier, while the probe is a supercontinuum white-light pulse. The differential transmission signal induced by the pump laser pulses is almost exclusively attributed to photoexcited electrons, while holes do not contribute, due to the peculiar electronic level structure of CdSe and CdS nanocrystals, where hole states are closely spaced together and the states at the very top of the valence band are not coupled to optical transitions.[45] Care was taken to avoid nonlinear effects due to multiple excitation of each nanocrystal by each laser pulse; laser fluence for such measurements is 0.6 μJ cm^{-2}, corresponding to an average of 0.7 excitations per nanocrystal per pulse. In order to exclude that the Pt decoration procedure introduces surface trap states that can lead to similar photophysical signatures as electron capture by Pt domains, we pre-treat Pt-free nanocrystals in the same hot bath used for Pt decoration, without adding Pt precursors (see the ESI† for details on the effects of such treatment).

The differential transmission traces in Fig. 3a are shown as a function of the pump–probe delay, so they reproduce the temporal dynamics of photoexcited electrons in the nanocrystals: Pt tipping accelerates the electron decay with respect to Pt-free nanocrystals, meaning that electrons can be trapped at the tips in a time scale of few hundreds of ps; a fit to a single exponential decay without constant background gave characteristic times of (630 ± 50) ps for Pt-free nanocrystals and (260 ± 30) ps for Pt-tipped nanocrystals. When the nanocrystals are entirely covered by Pt, however, the electron capture becomes much faster and is almost complete in a ~1 ps timescale, as shown in the zoom of the initial decay in Fig. 3b.

Differential transmission spectra, in Fig. 3c, reveal the photophysical processes. In Pt-free octapods and in tipped octapods the differential transmission spectra show similar dynamics: at time zero, just after excitation with the pump pulse, the bleaching is centered at 480 nm in wavelength, which has been associated with Scotognella and coworkers to the 1D electron state delocalized along the pod;[46,47] after a short transient of ~1–2 ps, the bleaching shifts towards the red and the corresponding peak moves to around 495 nm, a wavelength associated with the 0D electron state localized in the center of the nanocrystal. Such dynamics is the signature of energy relaxation of photoexcited electrons from higher to lower energy states in the conduction band, accompanied by a spatial migration from the pods (1D states) toward the nanocrystal center (0D states).[46] 0D states are localized not by a band potential, but mainly by a geometric effect,[46] as the nanocrystal cross-section is larger in the core than in the pods and the corresponding confining energy is lower. Therefore 0D states would exist even in nanocrystals with a CdS core and extend well within the CdS arms. Such localization is shallow, as the difference in energy between 0D and 1D states is around 70 meV, the effective mass for electrons is just 0.1 and thermal energy k_BT is at least 26 meV.

Relaxation is very similar in Pt-free and Pt-tipped nanocrystals because electron capture in tipped nanocrystals is a much slower process than energy relaxation, which is completed in ~1 ps. As a consequence, electron capture in Pt-tipped nanocrystals occurs from the 0D states, mostly localized in the center, which have little spatial overlap with the Pt domains located on the opposite side of the pods. As the localization of 0D states is mild, electron capture could be characterized as a tunneling through a shallow barrier.

The photoinduced absorption band at 460 nm is attributed to the Stark effect, *i.e.* the electric field created upon the excitation of electrons and holes that do not have a perfect spatial overlap. The Stark signal is expected to scale as a combination of the first and second derivative of the absorption spectrum and is therefore more pronounced in the samples where the absorption features are sharper, *i.e.*, in Pt-free octapods.

In Pt-covered nanocrystals, relaxation from 1D to 0D states does not occur, as the bleaching of the 0D state always dominates over the one corresponding to the 1D state, even immediately after excitation. Furthermore, combining the differential transmission with the absorbance spectra in Fig. 2b, we can calculate the peak in the transient absorption signal ($\Delta\alpha/\alpha_0$) to be about 4 times lower in Pt-covered nanocrystals than in Pt-free and Pt-tipped ones, where instead the values are about the same. We interpret the observation as an indication that bleaching in Pt-covered nanocrystals is only due to the fraction of electrons that after excitation directly relaxes into the 0D state, without transiting by the 1D states; on the other hand, we infer that electrons in the 1D states are captured by Pt domains before relaxation occurs, while they are still hot. In other words, electron capture in Pt-covered nanocrystals is fast enough to compete with energy relaxation. Since relaxation into the 1D states appears instantaneous in Pt-free nanocrystals, we also infer that electron capture in Pt-covered nanocrystals is faster even than the laser pump pulse duration.

Transient absorption tracks photoexcited electrons, but is mostly blind to photoexcited holes. To complete our

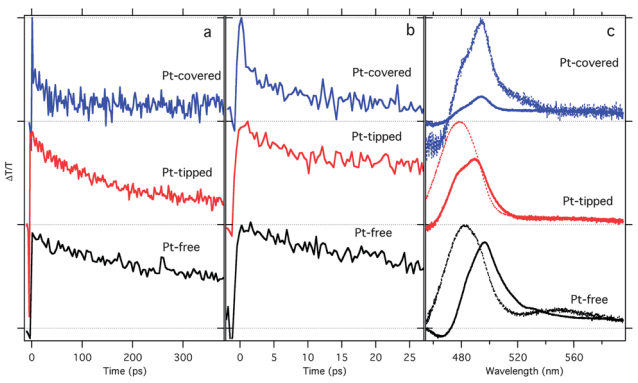

Fig. 3 (a) Decay of the spectrally integrated differential transmission signal as a function of pump–probe delay for CdSe@CdS octapod nanocrystals with different Pt decorations; the spectral integration window is 460–520 nm; signal amplitudes are normalized and vertically displaced for clarity. (b) Zoom of the initial decay. (c) Corresponding differential transmission spectra; the dotted lines are the spectra at time delay equal to zero (integrated over a 400 fs window), the continuous lines are the spectra integrated between 7 ps and 20 ps delay times.

photophysical investigation, we employ time-resolved photoluminescence, a technique that is sensitive to the simultaneous presence of electrons and holes. CdSe/CdS octapod nanocrystals are known as inefficient emitters, contrary to other CdSe/CdS colloidal nanostructures, as spherical core/shell and dot/rods. The low photoluminescence quantum yield may be related to the peculiar synthesis technique, which involves cation exchange of the original Cu_2Se core to produce the CdSe seed for nucleation of the eight CdS arms, a procedure that may leave potential barriers and crystal defects at the CdSe/CdS interface, inhibiting the relaxation of holes into the CdSe core. As a consequence the optical emission from octapod nanocrystals does not occur from the CdSe core, but from the CdS arm, and is centered in wavelength around 480 nm, as shown in Fig. 4a. The emission spectrum is slightly blueshifted in Pt-tipped and Pt-covered nanocrystals. The photoluminescence of Pt-free octapod nanocrystals decays in ~100 ps, a value close to the resolution of our streak camera; since transient absorption indicates a longer lifetime for electrons, we attribute the photoluminescence decay to hole trapping at the CdS surface. The photoluminescence dynamics is different in Pt-tipped and Pt-covered nanocrystals, as the decay becomes longer. It has to be noted however that the longer photoluminescence decay is not accompanied by a higher quantum yield; in contrast the quantum yield stays below 1% in all samples and is about 3 times lower in Pt-tipped and Pt-covered nanocrystals than in the Pt-free ones. This observation is consistent with transient absorption showing that the lifetime of electrons inside the nanocrystals is shortened by the addition of Pt. However, the timescales involving electron capture and photoluminescence decay are different by at least one order of magnitude, therefore we do not quantitatively link the quantum yield value to the electron capture rate: electron capture in Pt-tipped and Pt-covered nanocrystals may have different rates, but after few hundred ps, the total number of electrons that has been captured and therefore subtracted from photoluminescence may be similar, resulting in a comparable PL quantum yield. We infer that the treatment employed for Pt decoration affects the hole surface traps, probably saturating the deepest ones and therefore slowing down the hole recombination (further data on the effects of the decoration procedure on hole traps can be found in the ESI†).

All ultrafast optical measurements presented in Fig. 3 and 4 have been performed in the linear regime, with the pump fluence low enough to ensure that the transient absorption dynamics do not depend on the excitation level. Fig. 5 instead compares the differential transmission signals in Pt-free, Pt-tipped and Pt-covered nanocrystals as a function of the excitation fluence in the high-excitation regime, where every single

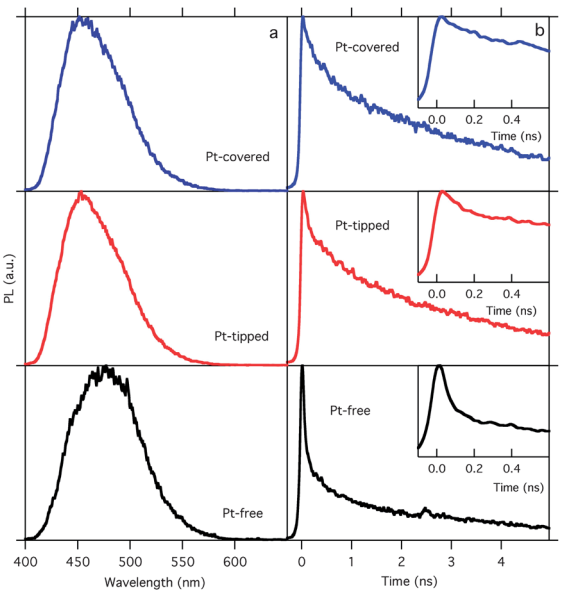

Fig. 4 (a) Photoluminescence spectra acquired with the streak camera for octapod nanocrystals. (b) Corresponding temporal decay of the normalized photoluminescence signal; spectral integration is done over the whole photoluminescence spectrum, 400–600 nm. Vertical displacements are for clarity. The insets show a magnification of the initial photoluminescence transient.

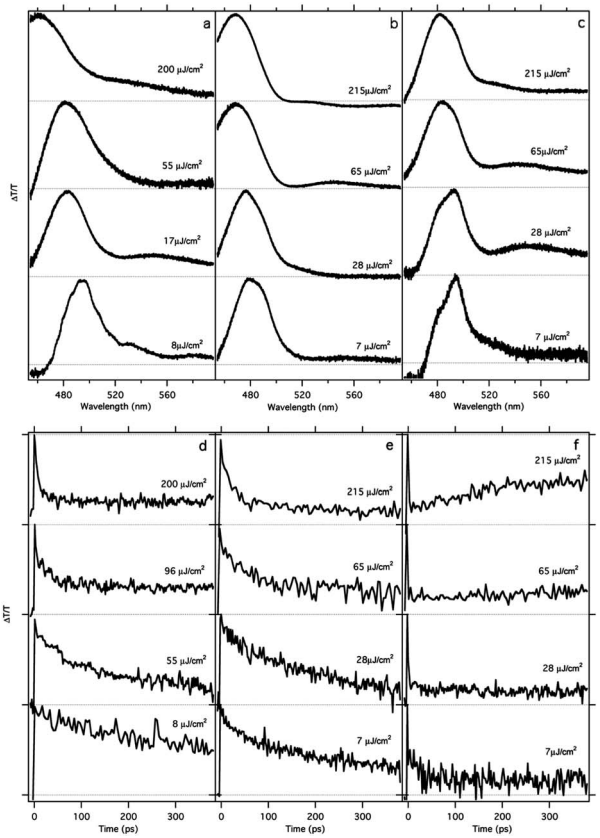

Fig. 5 (a–c) Differential transmission spectra as a function of laser fluence for CdSe@CdS octapod nanocrystals with a varying amount of Pt coverage: (a) Pt-free, (b) Pt-tipped, (c) Pt-covered; the spectra are integrated over a 2 ps window. (d–f) Corresponding dynamics of the differential transmission signals as a function of the delay time between pump and probe pulses: (d) Pt-free, (e) Pt-tipped, and (f) Pt-covered. The spectral integration window is 450–520 nm. 10 μJ cm^{-2} in excitation fluence corresponds to an average of 11.8 excitations per nanocrystal per pulse for Pt-free nanocrystals. Vertical displacements are for clarity.

laser pulse is intense enough to inject many photoexcitations into each nanocrystal (note that even the lowest laser fluence in Fig. 5 is much higher than what was employed in the linear measurements in Fig. 3 and 4).

In Pt-free nanocrystals (Fig. 5a), as the excitation fluence is increased, the bleaching signal blue-shifts as higher-energy transitions that are increasingly filled up with photoexcitations. Increasing the excitation level also produces a faster decay (Fig. 5d), a signature of non-radiative Auger recombination occurring when many photoexcitations are confined inside the same nanocrystal.[48] The Auger decay rate increases for increasing excitation levels, as the growing number of excitations coexisting in the same nanocrystal enhances the rates of scattering among carriers.

State filling and blue-shift of bleaching for increasing pump fluence are also apparent in the differential transmission spectra of Pt-tipped nanocrystals, as shown in Fig. 5b, but they are less pronounced than in Pt-free nanocrystals. We attribute such difference to the fact that, even in the multiple excitation regime, a large fraction of the photoexcited electrons is ejected from the nanocrystals due to the Pt decoration. The temporal dynamics in Fig. 5e confirms a shortening of the differential transmission decay in tipped nanocrystals for growing excitation levels, which can be linked to Auger recombination. However such shortening is modest in magnitude and, for the highest excitation levels we employ, the differential transmission decay turns out to be longer than in the corresponding Pt-free nanocrystals. We infer that the Pt tips reduce the Auger scattering rates, probably by promoting spatial charge separation even at very early times after excitation, when photoexcited electrons are still inside the nanocrystals.

In Pt-covered nanocrystals (Fig. 5c and f), the amplitude of the differential transmission signal decays rapidly, even at low excitation intensities, not because of Auger recombination, but due to fast electron capture by Pt domains. For growing pump fluences, the blueshift of the differential transmission signal shows that 1D states in the CdS pods are filled at comparably much higher excitation levels with respect to Pt-tipped nanocrystals, which we interpret as a confirmation of the fact that charges are separated and photoexcited electrons extracted from the nanocrystals before contributing to the bleaching signal in the semiconductor. A spectrally flat bleaching signal also appears at longer wavelengths and grows for growing pump fluences, which we attribute to excitation of plasmon modes in Pt domains.[45]

If the final goal of nanocrystal decoration with noble metals is to make them suitable for photocatalysis, Pt-decorated octapods appear very promising. The shape of such nanocrystals offers several distinctive advantages for photocatalytic applications, namely controlled charge separation and large absorption coefficients. Even more important, the absorption cross-section is very high, as much as 5×10^{-13} cm^2 at 500 nm in wavelength, meaning that under AM 1.5 solar illumination photoexcitations in each nanocrystal can be created at rates equal to 10^5 s^{-1}. Future studies with nanocrystals in hydrogen-production conditions will have to establish what is the best condition to maximize water splitting efficiency: selective Pt tipping of nanocrystals provides control over the spatial separation between electrons and holes while minimizing the amount of noble metal employed; on the other hand, non-selective Pt coverage of the CdS surface leads to faster charge separation, but may be less efficient in catalyzing reactions or more prone to unwanted recombination paths leading to back reactions.

Conclusions

In conclusion, we have demonstrated controlled deposition of Pt domains on CdSe@CdS octapod nanocrystals, synthesizing both selectively tipped and unselectively covered nanocrystals. Our measurements show that electron capture by Pt tips occurs in ~200 ps, providing just a perturbation to the excited state dynamics, while in Pt-covered nanocrystals electron capture is much faster, ~1 ps, and competes with energy relaxation and Auger recombination, causing the capture of hot electrons. Injection of multiple excitons into each nanocrystal results in the simultaneous charge separation by Pt domains of tens of electrons available for chemical reactions.

Acknowledgements

Work in Cagliari was partially funded by the Regione Autonoma della Sardegna through PO-FSE Sardegna 2007–2013, L.R. 7/2007, "Progetti di ricerca di base e orientata", Project no. CRP3-114, CRP-17571, CRP-18353, CRP-18013, and CRP-24978. L. Manna acknowledges the European Union's Seventh Framework Programme FP7/2007–2013 through grant agreement no. 240111 (starting ERC Grant NANO-ARCH). We acknowledge Dr A. Mattoni and Dr A. Falqui for fruitful discussions.

Notes and references

1 M. D. Archer and A. J. Nozik, *Nanostructured and photoelectrochemical systems for solar photon conversion*, Imperial College Press, London, 2008.
2 E. H. Sargent, *Nat. Photonics*, 2012, **6**, 133–135.
3 P. V. Kamat, *J. Phys. Chem. Lett.*, 2013, **4**, 908–918.
4 M. Graetzel, R. A. J. Janssen, D. B. Mitzi and E. H. Sargent, *Nature*, 2012, **488**, 304–312.
5 D. V. Talapin, J.-S. Lee, M. V. Kovalenko and E. V. Shevchenko, *Chem. Rev.*, 2010, **110**, 389–458.
6 L. Carbone and P. D. Cozzoli, *Nano Today*, 2010, **5**, 449–493.
7 *Semiconductor Nanocrystal Quantum Dots: Synthesis, Assembly, Spectroscopy and Applications*, ed. A. Rogach, Springer, 1st edn, 2010.
8 A. Vaneski, A. S. Susha, J. Rodriguez-Fernandez, M. Berr, F. Jäckel, J. Feldmann and A. L. Rogach, *Adv. Funct. Mater.*, 2011, **21**, 1547–1556.
9 C. A. Grimes, O. K. Varghese and S. Ranjan, *Light, Water, Hydrogen: The Solar Generation of Hydrogen by Water Photoelectrolysis*, Springer, 1st edn, 2007.
10 M. G. Walter, E. L. Warren, J. R. McKone, S. W. Boettcher, Q. Mi, E. A. Santori and N. S. Lewis, *Chem. Rev.*, 2010, **110**, 6446.

11 Y. Tachibana, L. Vayssieres and J. R. Durrant, *Nat. Photonics*, 2012, **6**, 511.
12 *Photoelectrochemical Hydrogen Production*, ed. R. Van de Krol and M. Graetzel, Springer Science+Business Media, 2012.
13 D. J. Milliron, S. Hughes, Y. Cui, L. Manna, J. Li, L. Wang and A. P. Alivisatos, *Nature*, 2004, **430**, 190–195.
14 H. Li, A. G. Kanaras and L. Manna, *Acc. Chem. Res.*, 2013, **46**, 1387–1396.
15 S. Deka, K. Miszta, D. Dorfs, A. Genovese, G. Bertoni and L. Manna, *Nano Lett.*, 2010, **10**, 3770–3776.
16 M. R. Kim, K. Miszta, M. Povia, R. Brescia, S. Christodoulou, M. Prato, S. Marras and L. Manna, *ACS Nano*, 2012, **6**, 11088–11096.
17 R. Brescia, K. Miszta, D. Dorfs, L. Manna and G. Bertoni, *J. Phys. Chem. C*, 2013, **115**, 20128–20133.
18 T. Mokari, E. Rothenberg, I. Popov, R. Costi and U. Banin, *Science*, 2004, **304**, 1787–1790.
19 T. Mokari, C. G. Sztrum, A. Salant, E. Rabani and U. Banin, *Nat. Mater.*, 2005, **4**, 855–863.
20 A. E. Saunders, I. Popov and U. Banin, *J. Phys. Chem. B*, 2006, **110**, 25421–25429.
21 S. E. Habas, P. Yang and T. Mokari, *J. Am. Chem. Soc.*, 2008, **130**, 3294–3295.
22 L. Amirav and A. P. Alivisatos, *J. Phys. Chem. Lett.*, 2010, **1**, 1051–1054.
23 M. Berr, A. Vaneski, A. S. Susha, J. Rodriguez-Fernandez, M. Döblinger, F. Jäckel, A. L. Rogach and J. Feldmann, *Appl. Phys. Lett.*, 2010, **97**, 093108.
24 A. Figuerola, M. V. Huis, M. Zanella, A. Genovese, S. Marras, A. Falqui, H. W. Zandbergen, R. Cingolani and L. Manna, *Nano Lett.*, 2010, **10**, 3028–3036.
25 M. J. Berr, A. Vaneski, C. Mauser, S. Fischbach, A. S. Susha, A. L. Rogach, F. Jäckel and J. Feldmann, *Small*, 2012, **8**, 291–297.
26 H. Baida, D. Mongin, D. Christofilos, G. Bachelier, A. Crut, P. Maioli, N. Del Fatti and F. Vallée, *Phys. Rev. Lett.*, 2011, **107**, 057402.
27 D. Mongin, E. Shaviv, P. Maioli, A. Crut, U. Banin, N. Del Fatti and F. Vallée, *ACS Nano*, 2012, **6**, 7034–7043.
28 B. P. Khanal, A. Pandey, L. Li, Q. Lin, W. K. Bae, H. Luo, V. I. Klimov and J. M. Pietryga, *ACS Nano*, 2012, **6**, 3832–3840.
29 E. Shaviv, O. Schubert, M. Alves-Santos, G. Goldoni, R. Di Felice, F. Vallée, N. Del Fatti, U. Banin and C. Sönnichsen, *ACS Nano*, 2012, **5**, 4712–4719.
30 H. Schlicke, D. Ghosh, L.-K. Fong, H. L. Xin, H. Zheng and A. P. Alivisatos, *Angew. Chem., Int. Ed.*, 2013, **52**, 980–982.
31 S. M. Kim, S. J. Lee, S. H. Kim, S. Kwon, K. J. Yee, H. Song, G. A. Somorjai and J. Y. Park, *Nano Lett.*, 2013, **13**, 1352–1358.
32 J. Muller, J. M. Lupton, P. Lagoudakis, F. Schindler, R. Koeppe, A. L. Rogach, J. Feldmann, D. V. Talapin and H. Weller, *Nano Lett.*, 2005, **5**, 2044–2049.
33 D. Steiner, D. Dorfs, U. Banin, F. Della Sala, L. Manna and O. Millo, *Nano Lett.*, 2008, **8**, 2954–2958.
34 M. G. Lupo, F. Della Sala, L. Carbone, M. Zavelani-Rossi, A. Fiore, L. Lüer, D. Polli, R. Cingolani, L. Manna and G. Lanzani, *Nano Lett.*, 2008, **8**, 4582–4587.
35 M. Saba, S. Minniberger, F. Quochi, J. Roither, M. Marceddu, A. Gocalinska, M. V. Kovalenko, D. V. Talapin, W. Heiss, A. Mura and G. Bongiovanni, *Adv. Mater.*, 2009, **21**, 4942–4946.
36 E. Yoskovitz, G. Menagen, A. Sitt, E. Lachman and U. Banin, *Nano Lett.*, 2010, **10**, 3068–3072.
37 M. G. Lupo, F. Scotognella, M. Zavelani-Rossi, G. Lanzani, L. Manna and F. Tassone, *Phys. Chem. Chem. Phys.*, 2012, **14**, 7420–7426.
38 L. T. Kunneman, M. Zanella, L. Manna, L. D. A. Siebbeles and J. M. Schins, *J. Phys. Chem. C*, 2013, **117**, 3146–3151.
39 J. Muller, J. M. Lupton, A. L. Rogach, J. Feldmann, D. V. Talapin and H. Weller, *Phys. Rev. B: Condens. Matter*, 2005, **72**, 205339.
40 N. J. Borys, M. J. Walter, J. Huang, D. V. Talapin and J. M. Lupton, *Science*, 2010, **330**, 1371–1374.
41 E. Shafran, N. J. Borys, J. Huang, D. V. Talapin and J. M. Lupton, *J. Phys. Chem. Lett.*, 2013, **4**, 691–697.
42 C. She, G. W. Bryant, A. Demortière, E. V. Shevchenko and M. Pelton, *Phys. Rev. B: Condens. Matter*, 2013, **87**, 155427.
43 M. Saba, M. Aresti, F. Quochi, M. Marceddu, M. A. Loi, J. Huang, D. V. Talapin, A. Mura and G. Bongiovanni, *ACS Nano*, 2013, **7**, 229–238.
44 D. Polli, L. Lüer and G. Cerullo, *Rev. Sci. Instrum.*, 2007, **78**, 103108.
45 *Semiconductor and Metal Nanocrystals: Synthesis and Electronic and Optical Properties (Optical Science and Engineering)*, ed. V. I. Klimov, CRC Press, 1st edn, 2003.
46 F. Scotognella, K. Miszta, D. Dorfs, M. Zavelani-Rossi, R. Brescia, S. Marras, L. Manna, G. Lanzani and F. Tassone, *J. Phys. Chem. C*, 2011, **115**, 9005–9011.
47 M. R. Antognazza, F. Scotognella, K. Miszta, D. Dorfs, M. Zanella, M. Zavelani-Rossi, L. Manna, G. Lanzani and F. Tassone, *Phys. Chem. Chem. Phys.*, 2011, **13**, 15326–15330.
48 V. I. Klimov, A. Mikhailovsky, D. McBranch, C. A. Leatherdale and M. G. Bawendi, *Science*, 2000, **287**, 1011–1013.